Activation of NF-κB signaling regulates ovariectomy-induced bone loss and weight gain

黄, 菲

BBA - Molecular Basis of Disease 1870 (2024) 167320

Contents lists available at ScienceDirect

BBA - Molecular Basis of Disease

journal homepage: www.elsevier.com/locate/bbadis

Activation of NF-κB signaling regulates ovariectomy-induced bone loss and weight gain

Fei Huang [a], Jing Gao [a], Aonan Li [a], Akiko Mizokami [b], Miho Matsuda [a], Kazuhiro Aoki [c], Takenobu Katagiri [d], Tomoyo Kawakubo-Yasukochi [b], Eijiro Jimi [a,b,*]

[a] Laboratory of Molecular and Cellular Biochemistry, Division of Oral Biological Sciences, Faculty of Dental Science, Kyushu University, 3-1-1 Maidashi, Higashi-ku, Fukuoka 812-8582, Japan
[b] Oral Health/Brain Health/Total Health Research Center, Faculty of Dental Science, Kyushu University, 3-1-1 Maidashi, Higashi-ku, Fukuoka 812-8582, Japan
[c] Department of Basic Oral Health Engineering, Graduate School, Tokyo Medical and Dental University, 1-5-45, Yushima, Bunkyo-ku, Tokyo 113-8549, Japan
[d] Division of Biomedical Sciences, Research Center for Genomic Medicine, Saitama Medical University, Hidaka-shi, Saitama 350-1241, Japan

ARTICLE INFO

Keywords:
Postmenopausal osteoporosis
NF-κB activation
Weight gain
Glucose tolerance
Bone loss
Disulfiram

ABSTRACT

Postmenopausal women experience bone loss and weight gain. To date, crosstalk between estrogen receptor signals and nuclear factor-κB (NF-κB) has been reported, and estrogen depletion enhances bone resorption by osteoclasts via NF-κB activation. However, it is unclear when and in which tissues NF-κB is activated after menopause, and how NF-κB acts as a common signaling molecule for postmenopausal weight gain and bone loss. Therefore, we examined the role of NF-κB in bone and energy metabolism following menopause. NF-κB reporter mice, which can be used to measure NF-κB activation in vivo, were ovariectomized (OVX) and the luminescence intensity after OVX increased in the metaphyses of the long bones and perigonadal white adipose tissue, but not in the other tissues. OVX was performed on wild-type (WT) and p65 mutant knock-in (S534A) mice, whose mutation enhances the transcriptional activity of NF-κB. Weight gain with worsening glucose tolerance was significant in S534A mice after OVX compared with those of WT mice. The bone density of the sham group in WT or S534A mice did not change, whereas in the S534A-OVX group it significantly decreased due to the suppression of bone formation and increase in bone marrow adipocytes. Disulfiram, an anti-alcoholic drug, suppressed OVX-induced activation of NF-κB in the metaphyses of long bones and white adipose tissue (WAT), as well as weight gain and bone loss. Overall, the activation of NF-κB in the metaphyses of long bones and WAT after OVX regulates post-OVX weight gain and bone loss.

1. Introduction

The world is rapidly becoming a super-aging society, and women spend nearly one-third of their lives in the menopausal state. The depletion of sex hormones is an important consequence of normal aging and gonadal failure [1–3]. Estrogen is the main female sex hormone, and it has been established that postmenopausal women experience a decrease in bone mass. However, estrogen deficiency also increases the risk of developing various diseases such as dyslipidemia, metabolic syndrome, and breast cancer specific to women [1–3]. A decline in bone

Abbreviations: NF-κB, Nuclear factor-κB; OVX, ovariectomy; WT, wild type; WAT, white adipose tissue; DSF, disulfiram; TNF-α, tumor necrosis factor α; ER, Estrogen receptor; RANKL, receptor activator of NF-κB ligand; HFD, high-fat diet; MEF, mouse embryonic fibroblast; M-CSF, macrophage colony-stimulating factor; SPF, specific pathogen-free; ELISA, enzyme-linked immunosorbent assay; pgWAT, perigonadal white adipose tissue; H&E, Mayer's hematoxylin and eosin Y; BV/TV, bone volume/tissue volume; Tb.N, trabecular number; Tb.Sp, trabecular separation; Tb.Th, trabecular thickness; N.Oc/BS, osteoclast number/bone surface; ES/BS, eroded surface/bone surface; TRAP, tartrate-resistant acid phosphatase; MNC, multinucleated cell; BFR, bone formation rate; MS/BS, mineralized surface/bone surface; MAR, mineral apposition rate; GTT, glucose tolerance test; ITT, insulin tolerance test; CTX-I, C-terminal telopeptide of collagen type I; 3D, three-dimensional; BMD, bone mineral density; BMSC, bone marrow mesenchymal stem cell; β-GP, β-glycerophosphate; A.A, ascorbic acid; ALP, alkaline phosphatase; BAT, brown adipose tissue; HOMA-IR, Homeostatic Model Assessment for Insulin Resistance; AUC, area under the curve; IL-6, interleukin-6; IL-1β, interleukin-1β; ALDH, aldehyde dehydrogenase; MetS, metabolic syndrome; PAI-1, plasminogen activator inhibitor 1.

* Corresponding author at: Oral Health/Brain Health/Total Health Research Center, Faculty of Dental Science, Kyushu University, 3-1-1 Maidashi, Higashi-ku, Fukuoka 812-8582, Japan.
E-mail address: ejimi@dent.kyushu-u.ac.jp (E. Jimi).

https://doi.org/10.1016/j.bbadis.2024.167320
Received 14 March 2024; Received in revised form 13 June 2024; Accepted 19 June 2024
Available online 25 June 2024

density increases the risk of fractures and the need for nursing care. Central obesity due to estrogen deficiency is thought to be an early stage of diseases related to metabolic syndrome. Accumulated visceral fat secretes inflammatory cytokines, such as interleukin-6 (IL-6) and tumor necrosis factor α (TNF-α), inducing insulin resistance [4]. Thus, examining the mechanisms underlying postmenopausal bone loss and metabolic diseases is important for improving the quality of life for women.

Estrogen binds to two types of estrogen receptors (ER), ERα and ERβ, and the estrogen/estrogen receptor complexes act as transcription factors. Both subtypes are expressed in different tissues and cells in humans, regulating important physiological functions in several organ systems, including the reproductive, cardiovascular, skeletal, and central nervous However, it has been reported that estrogen also exerts nongenomic actions that are not mediated by these nuclear receptors [5]. Meanwhile, the transcription factor NF-κB regulates biological phenomena such as inflammatory responses, immune responses, cell proliferation/survival, and apoptosis, and is activated by various cytokines and UV irradiation-induced stress [6–8]. The mutually antagonistic crosstalk between NF-κB and the ER signaling pathway has been well studied. This crosstalk is particularly related to bone metabolism; estrogen deficiency induces the expression of receptor activator of NF-κB ligand (RANKL) in osteoblastic cells, an osteoclast differentiation factor, and promotes bone resorption by osteoclasts [11]. Furthermore, many research groups, including ours, have shown that either pharmacological or genetic inhibition of NF-κB suppresses bone resorption by osteoclasts, thereby suppressing bone destruction in disease models where bone resorption is accelerated, such as osteoporosis, periodontitis, and arthritis [12–15]. NF-κB is also important for regulating energy metabolism, and it has been reported that suppressing NF-κB specifically in the hypothalamus, liver, or adipose tissue prevents high-fat diet (HFD)-induced obesity and deterioration of carbohydrate and lipid metabolism [16–18]. Therefore, we considered the possibility that NF-κB activation is involved not only in postmenopausal bone loss but also in weight gain.

Activation of NF-κB occurs when IκB kinase is activated by extracellular stimulation, and IκB is phosphorylated and degraded, which results in the translocation of a heterodimer of NF-κB1 (p50) and RelA (p65) to the nucleus and induces the expression of target genes [6–8]. Recently, a new regulatory mechanism based on the phosphorylation of the RelA subunit has been reported. It has been reported that there are many phosphorylation sites in the RelA subunit [19,20]. There are many studies regarding the phosphorylation of serine residue 536 in humans (534 in mice), but their physiological functions are unclear [21]. Therefore, Pradère et al. [22] and our research group independently established knock-in (S534A) mice in which serine residue 534 was replaced with alanine. S534A mice developed normally, and detailed histological analysis of the lungs, liver, thymus, spleen, and pancreas, which showed marked S534 phosphorylation, revealed no abnormalities. Furthermore, when mouse embryonic fibroblasts (MEFs) derived from S534A mice were stimulated with TNF-α, the duration of binding to the κB motif was longer and transcriptional activity was higher than those in MEFs derived from wild-type (WT) mice [22]. Based on these results, the phosphorylation of S534 was considered to negatively regulate transcriptional activity, and S534A mice were considered a model wherein NF-κB transcriptional activity increased in a stimulus-dependent manner.

In this study, we first established reporter mice that express the luciferase gene under the control of the NF-κB response element to identify the tissues in which NF-κB is activated early by estrogen deficiency. Subsequently, ovariectomy (OVX) was performed and showed activation of NF-κB in the metaphyses of long bones and perigonadal white adipose tissue (pgWAT). Furthermore, the reporter mice were crossed with S534A mice, and NF-κB transcriptional activity was enhanced in the long bones and white adipose tissues (WATs) of S534A mice one week after OVX. Weight gain due to increased fat weight and insulin resistance was observed in the OVX group of S534A mice when WT and S534A mice were subjected to OVX. Furthermore, bone loss increased in the OVX group of S534A mice, which was attributed to the suppression of bone formation. We also selected anti-alcoholic drug disulfiram (DSF) as a candidate drug for the treatment of bone loss and weight gain induced by estrogen deficiency because it suppresses NF-κB activation [23], inhibits bone resorption [24], and improves obesity and energy metabolism [25]. DSF has been clinically applied with confirmed safety [26]. Finally, subcutaneous administration of the DSF inhibited OVX-induced NF-κB activation, further inhibiting weight gain and bone loss. Overall, our findings suggest that estrogen deficiency induces the activation of NF-κB in long bone metaphyses and WAT, and the degree of NF-κB activation may modulate postmenopausal bone loss and weight gain.

2. Methods

2.1. Reagents

Glutathione S-transferase (GST)-RANKL was obtained from the Oriental Yeast Company, Ltd. (Shiga, Japan). Human macrophage-stimulating factor (M-CSF) was obtained from FUJIFILM Wako Pure Chemical Corporation (Osaka, Japan). The antibodies used, including anti-p-NF-κB p65 (Ser536) (#3033), anti-NF-κB p65 (#8242) and anti-adiponectin (#2789), were purchased from Cell Signaling Technology (Danvers, MA). Anti-β-actin (#AC-15) antibody was purchased from Merck Millipore (Darmstadt, Germany). DSF was purchased from Cayman Chemical Company (Ann Arbor, MI).

2.2. Mice

All procedures were approved by the Animal Care Committee of Kyushu University and were performed in accordance with the guidelines of the Japanese Council on Animal Care (approval number: A22-236-2, 24-264) and the Guidelines for Proper Conduct of Animal Experiments of the Science Council of Japan. All experiments were performed according to the ARRIVE guidelines. We generated a knock-in (S534A) mice, in which serine at position 534 (the murine homolog of human Ser 536) of the p65 subunit of NF-κB was replaced with alanine. The mice were maintained under specific pathogen-free (SPF) conditions with a 12-h light:12-h dark cycle. For all experiments, 9-week-old female C57BL/6J or S534A mice were subjected to OVX. After OVX, mouse body weight was monitored weekly at 15:00. Mice were euthanized after various weeks of OVX according to the experimental requirements. To measure food intake, singly housed mice were fed a normal diet. Blood for serum analysis was collected via the orbital plexus from mice anesthetized with sevoflurane. The serum was subsequently analyzed for insulin levels using enzyme-linked immunosorbent assay (ELISA) kits purchased from Fujifilm (633-03411). Serum glucose levels were measured using a D-glucose assay kit (GOPOD Format) (Megazyme, Chicago, IL).

Female C57BL/6 J mice were randomly divided into three groups to receive the following treatments: (1) sham group (sham operation +20 % DMSO in propylene glycol, $n = 8$), (2) OVX group (OVX + DMSO in propylene glycol, $n = 9$), and (3) OVX + DSF group (OVX operation + DSF, 50 mg/kg, $n = 9$). After 1 week of recovery from Sham or OVX, DSF and vehicle (propylene glycol) solution (e.g. 100 μL for 20 g weight of mouse) were administered subcutaneously every two days to mice for four weeks. After OVX, mouse body weight was monitored weekly at 15:00. After euthanasia, the femurs and pgWAT were isolated and collected.

The specific primers used for genotyping were as follows: κB-Luc F:5′-TATCCGCTGGAAGATGGAAC-3′; R:5′-TATCGAAGGACTCTGGCACA-3′; S534A F:5′-GCAACAGCACAGACCCAGGAGT-3′; and R:5′-CCCCAGAGA-GATCACCCAAACA-3′.

2.3. Bioluminescence imaging

NF-κB reporter mice carrying a transgene in which the five binding sites of NF-κB (5′-GGGAATTTCCG-3′) were directly linked to the luciferase gene under the control of a minimal promoter were used for ex vivo imaging (Supplementary Fig. 1A). Mice were intraperitoneally injected with d-luciferin (150 mg/kg) (PerkinElmer, Waltham, MA). Five minutes later, the mice were intraperitoneally anesthetized with medetomidine hydrochloride (0.75 mg/kg body weight, Kyoritsu Seiyaku, Tokyo, Japan), midazolam (4 mg/kg, Fuji Pharma, Tokyo, Japan), and butorphanol tartrate (5 mg/kg, Meiji Seika Pharma, Tokyo, Japan). The brain, thymus, lung, liver, spleen, muscles, bones, pgWAT, and brown adipose tissue (BAT) were isolated, and bioluminescence signals were obtained using an IVIS Spectrum (PerkinElmer). The bioluminescence signal data were quantified using Living Image version 4.3.1 (Caliper Life Sciences). ROIs were plotted in the femur or pgWAT region for each experiment.

2.4. Histological Analysis and bone histomorphometry

For paraffin section preparation, pgWAT and femurs were isolated and fixed in 4 % paraformaldehyde in 0.1 M phosphate buffer (pH 7.2). Femurs were further decalcified using Osteosoft (Merck Millipore). The fixed tissues were dehydrated in a series of ethanol solutions and embedded in paraffin. Paraffin sections were prepared with a thickness of 5 μm and stained with Mayer's hematoxylin and eosin Y (H&E) (Sakura Finetek, Tokyo, Japan) according to standard procedures. Images were acquired using an all-in-one fluorescence Microscope BZ-X800 (Keyence, Osaka, Japan). The adipocyte area was evaluated in three representative fields per section using the BZ-Analyzer-II software (Keyence).

Femoral sections were analyzed using tartrate-resistant acid phosphatase (TRAP) staining and counterstained with methyl green. Osteoclasts are $TRAP^{+}$ multinucleated cells (MNCs) containing three or more nuclei in the bone marrow [13].

Frozen, decalcified femoral sections were prepared for Oil Red O staining. After fixation and decalcification, the femurs were dehydrated with gradient sucrose solutions at 4 °C, followed by embedding in OCT compound (Sakura Finetek). The frozen sections were cut at a thickness of 5 μm and rinsed with distilled water and replaced by 60 % isopropanol. Oil Red O staining was conducted using Oil Red-O solution (Merck Millipore) in 60 % isopropanol for 30 min, followed by counterstaining with methyl green. The slides were then washed thoroughly with distilled water.

To analyze the rate of bone formation, mice were intraperitoneally administered calcein (20 mg/kg, Sigma) at 10 days and Alizarin Complexone (20 mg/kg, TCI) 2 days before sacrifice. Femurs were isolated and fixed without decalcification. Femurs were embedded in Super Cryoembedding Medium compound (SCEM; Section-Lab Co. Ltd., Hiroshima, Japan) and subsequently frozen into blocks at −100 °C using a freezing machine (UT2000F; Leica Microsystems, Tokyo, Japan). The undecalcified frozen blocks were then cut into slices of 5 μm thickness using a microtome (CM1860 UV; Leica Microsystems) and attached to the adhesive Kawamoto film (Cryofilm type 2C, Section-Lab, Co., Ltd) following the Kawamoto method [27]. The bone formation rate (BFR), mineralized surface/bone surface (MS/BS), mineral apposition rate (MAR) in the distal regions of the femurs of mice, and eroded surface/bone surface (ES/BS, %) were measured as described previously [28].

2.5. Metabolic assessment

After the mice were fasted for 16 h, a glucose tolerance test (GTT) was performed [29]. Glucose (2 g/kg) was injected intraperitoneally and blood glucose concentrations were measured at different times using a handheld glucometer, FreeStyle Lite glucose test strips (Abbott Laboratories). To perform the insulin tolerance test (ITT), insulin (0.5 U/kg for mice 3 weeks after OVX, 0.25 U/kg for mice 7 weeks after OVX; Humulin R, Eli Lilly and Company, Indianapolis, IN, USA) was injected intraperitoneally after a 4-h fasting, and blood glucose concentrations were then measured at different times in the same way as described in the GTT. The HOMA-IR index was calculated as fasting serum glucose (mg/dl) × fasting serum insulin (ng/mL) × 26/405 [30].

2.6. Quantitative real-time PCR

Total RNA was extracted from pgWAT using the ReliaPrep RNA Tissue Miniprep Kit (Promega). Total RNA (1 μg) was reverse transcribed into cDNA using ReverTra Ace (Toyobo, Osaka, Japan). Quantitative RT-PCR analysis was performed using KOD SYBR qPCR Mix (TOYOBO, Osaka, Japan) in a Takara PCR Thermal Cycler Dice Gradient instrument (Takara Bio, Shiga, Japan). β-Actin was used as an internal control. The specific primers used were as follows: CD11c F:5′-GAGCCAGAACTTCCCAACTG-3′; R:5′-TCAGGAACACGATGTCTTGG-3′; IL-1β F:5′-TCGCTCAGGGTCACAAGAAA-3′; R:5′-CATCAGAGGCAAGGAGGAAAAC-3′; IL-6 F:5′-GCTACCAAACTGGATATAATCAGGA-3′; R:5′-CCAGGTAGCTATGGTACTCCAGAA-3′; TNF-α F:5′-TCTTCTCATTCCTGCTTGTGG-3′; R:5′-GGTCTGGGCCATAGAACTGA-3′; Adiponectin F:5′-TGTTCCTCTTAATCCTGCCCA-3′; R:5′-CCAACCTGCACAAGTTCCCTT-3′; Leptin F:5′-GAGACCCCTGTGTCGGTTC-3′; and R:5′-CTGCGTGTGTGAAATGTCATTG-3′.

2.7. Radiological assessments

After dissection, femurs were fixed in 4 % paraformaldehyde in 0.1 M phosphate buffer (pH 7.2). Femoral internal structure images were taken by a high-resolution microcomputed tomography (μCT; ScanXmate-L090T, Comscan Co, Kanagawa, Japan). Scans were acquired using an isotropic voxel size of 11.468 μm, an X-ray tube potential of 60 kVP, an X-ray tube intensity of 120 μA, and an integration time of 2 fps. After taking the femoral structural images, the three-dimensional (3D) structure of each sample was reconstructed and analyzed using the ConeCTexpress software (Comscan). The trabecular and cortical bones of femurs were analyzed with TRI/3D-BON (TRI) software (RATOC Systems) to calculate the bone mineral density, bone volume/tissue volume (BV/TV, %), trabecular number (Tb.N, /mm), trabecular separation (Tb.Sp, mm), trabecular thickness (Tb.Th, μm) using five hydroxyapatite standard curves of known density.

2.8. Detection of C-terminal telopeptide of collagen type I (CTX-I) in serum

The whole blood of WT and S534A mice was collected after 4 weeks of Sham and OVX, and the centrifuged supernatant was collected for immediate use or stored at −80 °C. CTX-1 in 20 μL of serum was measured using a Rat-Laps (CTX-I) EIA kit (AC-06F1, Immunodiagnostic Systems, Tyne and Wear, UK) according to the manufacturer's protocol.

2.9. Bone marrow mesenchymal cells (BMCs) preparation and differentiation

BMCs were isolated from femurs and tibiae of female C57BL/6J or S534A mice at 4 weeks of age or 4 weeks after Sham or OVX and cultured in α-minimal essential medium supplemented with 10 % fetal bovine serum, 100 units/mL penicillin, and 100 μg/mL streptomycin. For adipogenesis, BMCs were treated with dexamethasone (1 μM), troglitazone (10 μM), insulin (10 μg/mL), and IBMX (0.5 mM) for 6 days, followed by insulin (10 μg/mL) only for another 2 days. For osteoblast differentiation, BMCs were treated with β-glycerophosphate (β-GP) (10 mM) and ascorbic acid (A.A) (50 μg/mL) for 7 or 21 days.

2.10. Alkaline phosphatase activity and staining

To assess alkaline phosphatase (ALP) activity, cells were incubated with an ALP substrate buffer (10 mg/mL *p*-nitrophenyl phosphate, 0.1 M diethanol amine, and 1 mM MgCl2, pH 8.0) after fixing with an acetone/ethanol mixture (50:50, v/v). The reaction was stopped after 5 min by the addition of 5 M NaOH. Absorbance was measured at 405 nm using a microplate reader (Bio-Rad Laboratories Inc., Hercules, CA). ALP staining was performed with ALP staining solution (0.1 mg/mL naphthol AS-MX phosphate (Merck Millipore), 0.5 % *N*, *N*-dimethylformamide, 2 mM $MgCl_2$, and 0.6 mg/mL of fast blue BB salt (Merck Millipore) in 0.1 M Tris–HCl (pH 8.5)) for 15 min [31].

2.11. Alizarin red S staining

After fixation and thorough washing with distilled water, the cells were stained with 1 % Alizarin Red S solution for 30 min at 25 °C. For quantification, Alizarin red dye was dissolved in 10 % formic acid (ARDSET; PG Research, Tokyo, Japan), and the absorbance was measured at 405 nm using a microplate reader [31].

2.12. Immunoblotting

Cells differentiated from BMCs were lysed in ice-cold lysis buffer (50 mM Tris-HCl [pH 7.5], 150 mM NaCl, 5 mM EDTA, and 1 % Triton X-100). Cell lysates were fractionated using sodium dodecyl sulfate (SDS)-sulfate-polyacrylamide gels and transferred to PVDF membranes (Merck Millipore). Immunoblotting was performed as previously described [32]. The primary antibody was used at a dilution of 1:1000 (for anti-p-NF-κB p65, anti-NF-κB p65, and anti-adiponectin antibodies) or 1:5000 (for anti-β-actin antibody). The secondary antibody was used at a dilution of 1:5000. Digital images were obtained using the Amersham ImageQuant 800 system (Cytiva, Tokyo, Japan).

2.13. Statistical analysis

Quantitative data are presented as the mean ± SD. Means between the two groups were compared using the unpaired *t*-test (versus the control; * $p < 0.05$, ** $p < 0.01$). For comparisons involving more than two groups, two-way analysis of variance (ANOVA) with Tukey's test for multiple comparisons was employed. Significance levels were denoted as * $p < 0.05$, ** $p < 0.01$, *** $p < 0.001$, and **** $p < 0.0001$. Statistical analysis was conducted using Prism software package version 9.4.1 (GraphPad Software, Inc., San Diego, CA).

3. Results

3.1. Elevated NF-κB activity in femur and adipose tissue in S534A mice after OVX-surgery

To investigate in which tissues NF-κB is activated after OVX, 9-week-old female NF-κB reporter mice were subjected to Sham or OVX, and 1 week later, D-luciferin was administered intraperitoneally. The brain, thymus, lungs, liver, spleen, muscles, bones, pgWAT, and brown adipose tissue (BAT) were removed, and ex vivo imaging was performed. In the OVX group, luminescence was stronger in the femoral metaphyses and pgWAT, but there were no significant differences in other tissues compared to the sham group (Fig. 1A and B, Supplementary Fig. 1B).

Next, we crossed S534A mice with the NF-κB reporter mice (Supplementary Fig. 1A), performed Sham or OVX, and examined the activation of the NF-κB in the bone and pgWAT after 1 week. Compared with NF-κB reporter mice, stronger luminescence was detected in the femoral metaphyses and adipose tissue of S534A/NF-κB reporter mice (Fig. 1C and D). These results showed that the NF-κB activity was increased in the femoral metaphyses and WAT at 1 week after OVX, and the NF-κB activity was further enhanced in S534A mice.

3.2. Body weight gain and adipose tissue deposition in S534A mice after OVX-surgery

The body weights of WT and S534A females were measured weekly after surgery (Fig. 2A), with the results indicating that S534A-OVX mice gained significantly more body weight than WT-OVX mice from 4 weeks after surgery. In addition, a significant difference in body weight was observed between the WT-Sham and S534A-Sham mice at 21 weeks of age (12 weeks after sham surgery) (Fig. 2B). However, the food intake did not differ among the four groups (Supplementary Fig. 2A). Next, we investigated whether any changes in WAT weight occurred concurrently with differences in body weight. Four and 12 weeks after surgery, the ratio of pgWAT weight to body weight was significantly higher in S534A mice than that in WT mice under the same conditions (Fig. 2C and D). Histological analyses of pgWAT showed that the adipocyte area in S534A-Sham was larger than that in WT-Sham mice and that the degree of adipocyte increase caused by OVX was particularly pronounced in S534A mice between 4 and 12 weeks after surgery (Fig. 2E and F).

3.3. Insulin resistance in S534A mice

Next, we investigated glucose metabolism, insulin sensitivity, and insulin tolerance in S534A mice 3 or 4 weeks after Sham or OVX surgery. The area under the curve (AUC) values of the IPGTT was higher in the OVX group than in the control group (Fig. 3A). In contrast, in the ITT test, WT-OVX mice showed AUC values similar to those of WT-Sham mice (Fig. 3B). This is probably because they were fed a normal diet because HFD adversely affects insulin sensitivity [33]. Remarkably, insulin resistance was significantly observed in both the S534A-Sham and -OVX groups compared to the corresponding WT groups, as supported by the AUC values (Fig. 3B). The results of the IPGTT and ITT 7 or 8 weeks after surgery indicated a similar tendency (Supplementary Fig. 2C and D) to the results from 3 or 4 weeks after surgery, respectively (Fig. 3A and B). In particular, insulin resistance between the sham and OVX groups in S534A mice at 8 weeks after surgery became more pronounced (Supplementary Fig. 2D) compared with the results from 4 weeks after surgery (Fig. 3B).

Moreover, the HOMA-IR, which was calculated based on fasting glucose (Fig. 3C), and fasting insulin levels (Fig. 3D), was increased in S534A mice (Fig. 3E). These results indicated that impaired glucose metabolism, particularly insulin resistance, was markedly accelerated in S534A mice, which may also contribute to the abnormal glucose metabolism and obesity that occur in a state of ovarian-derived estrogen depletion.

It has been well-established that CD11c-positive M1 macrophages can induce inflammation and insulin resistance via the secretion of pro-inflammatory cytokines, such as TNF-α, IL-6, and interleukin-1β (IL-1β) in the adipose tissues [4]. Adipocytokines, such as adiponectin and leptin, are also associated with insulin resistance [34]. Therefore, we examined the expression of CD11c and adipose-related cytokines. As a result, we found that CD11c and the subsequent expression of TNF-α, but not IL-6 and IL-1β, were significantly increased in pgWAT of S534A-OVX mice compared with WT-OVX mice (Fig. 3F–I). The expression of adiponectin was decreased in the pgWAT of S534A-OVX mice compared to that in S534A-Sham mice (Fig. 3J). Meanwhile, no pronounced difference was observed in the expression levels of leptin between the groups (Fig. 3K). Given that TNF-α has been identified as a causative regulator of inflammation and insulin resistance in adipose tissues [35,36], these observations suggested that obesity and abnormal energy metabolism in S534A-OVX mice were triggered in these adipose tissues.

3.4. Bone loss due to inhibition of bone formation after OVX in S534A mice

Next, we compared bone loss after OVX in WT and S534A mice. Micro-CT images showed no difference in bone mineral density (BMD)

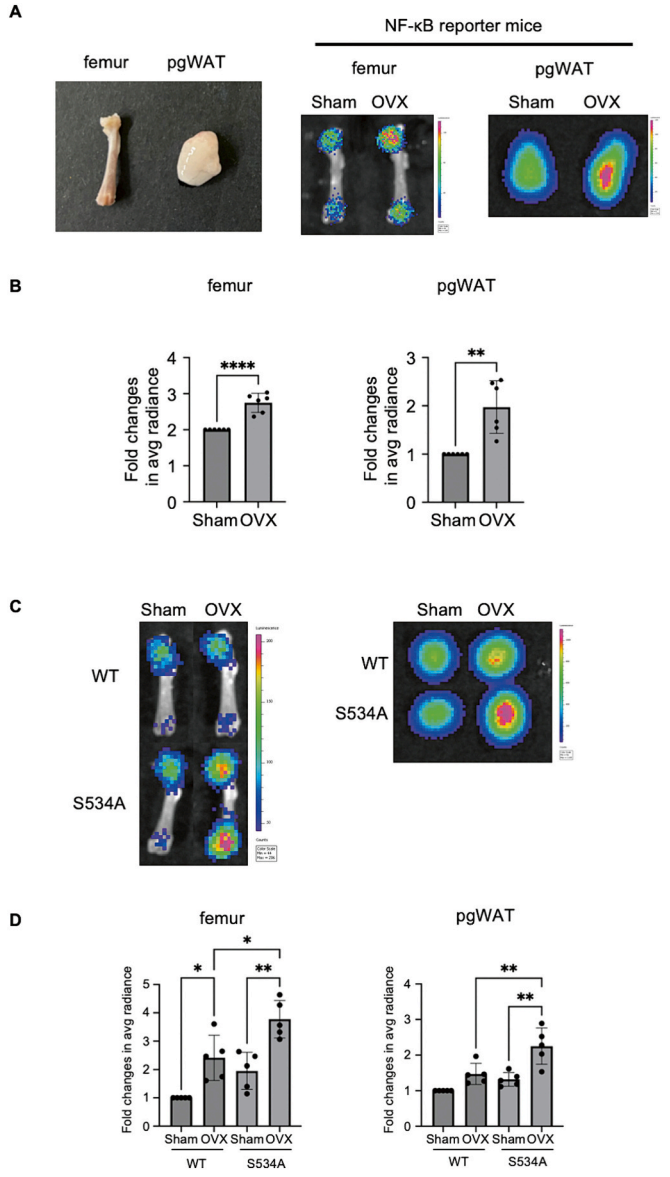

Fig. 1. Activation of NF-κB in bone and adipose tissue in S534A mice following OVX surgery. **A.** Nine-week-old female NF-κB reporter mice were subjected to sham or OVX surgery, and 1 week later, D-luciferin (150 mg/kg) was administered intraperitoneally. The luminescence intensity of the femur and pgWAT was measured using IVIS Spectrum. Representative images of luminescence intensity in femur and pgWAT 1 week after sham or OVX in 9-weeks-old female NF-κB reporter mice. **B.** Luminescence intensity was quantified and expressed as fold change ($n = 6$). All values are shown as the means ± SD. Statistical analysis between two groups was performed using unpaired *t*-test. **C.** Representative images of luminescence intensity in femur and pgWAT 1 week after sham or OVX in 9-week-old female NF-κB reporter mice or S534A/NF-κB reporter mice. **D.** Luminescence intensity was quantified and expressed as fold change ($n = 5$). All values are shown as the means ± SD. Statistical analysis among four groups was performed using two-way ANOVA followed by Tukey's post hoc test. $^{*}P < 0.05$, $^{**}P < 0.01$, $^{***}P < 0.001$.

between WT-Sham and S534A-Sham mice. A decrease in trabecular bone density, but not the cortical bone, was observed in the OVX group compared to the sham group of WT mice, but the density was further decreased in the OVX group of S534A mice (Fig. 4A–C). BV/TV, Tb.N, and Tb.Sp, but not Tb.Th, were also decreased in S534A-OVX mice compared to those in WT-OVX mice (Fig. 4D–G).

Bone morphometry was performed to determine whether the further decrease in bone density of S534A-OVX mice compared to that of WT-

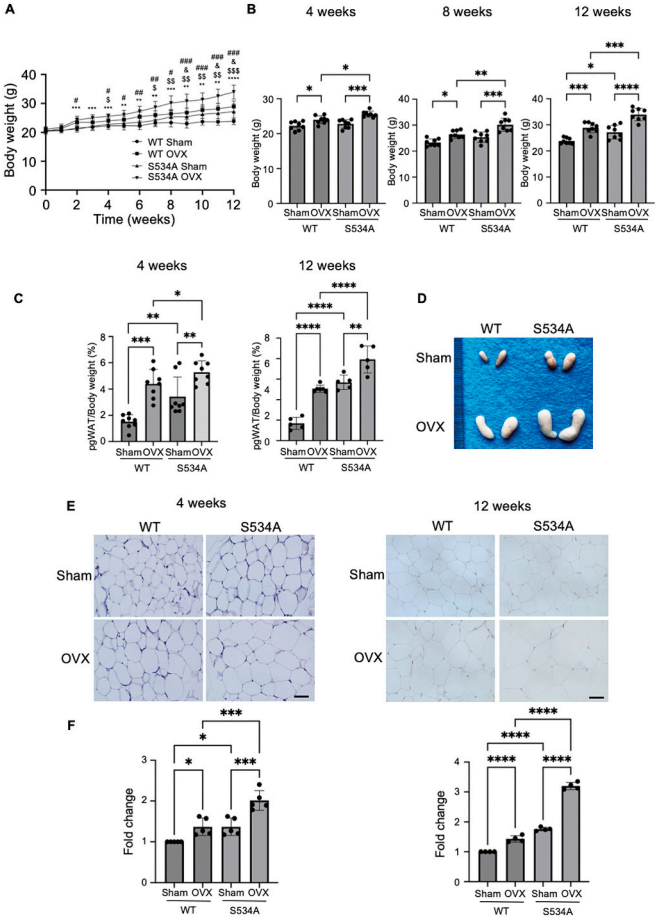

Fig. 2. Changes in body weight and the weight of adipose tissue in S534A mice following OVX surgery. **A, B.** Body weight of WT and S534A mice were measured weekly after sham or OVX operation at 9-weeks-old ($n = 8$). Growth curves (A) and body weight at 4, 8, and 12 weeks after sham or OVX (B). **C.** Ratios of pgWAT to body weight in WT and S534A mice 4, and 12 weeks after Sham or OVX (n = 5–8). **D.** Representative appearance of pgWAT. **E.** Representative images of H&E staining in pgWAT from WT and S534A mice 4 and 12 weeks after Sham or OVX. Scale bars: 50 μm. **F.** Quantification of the adipocyte area (area per adipocyte, μm^2) performed using a microscope at 40 x magnification in 3 random fields per section, and expressed as fold change ($n = 4–5$). All values are shown as the means ± SD. Statistical analysis was performed using two-way repeated measures ANOVA (A), WT Sham vs. WT OVX: $\#P < 0.05$, $\#\#P < 0.01$, $\#\#\#P < 0.001$, WT Sham vs. S534A Sham: $\&P < 0.05$, WT OVX vs. S534A OVX: $\$P < 0.05$, $\$\$P < 0.01$, $\$\$\$P < 0.001$, S534A Sham vs. S534A OVX: $^{*}P < 0.05$, $^{**}P < 0.01$, $^{***}P < 0.001$, $^{****}P < 0.0001$, two-way ANOVA followed by Tukey's post hoc test (B, C, F). $^{*}P < 0.05$, $^{**}P < 0.01$, $^{***}P < 0.001$, $^{****}P < 0.0001$.

OVX mice was due to enhanced bone resorption or suppression of bone formation. Since NF-κB inhibitors suppress bone loss after OVX by suppressing osteoclastic bone resorption [12,13], it had been expected that bone resorption would be further accelerated in the OVX group of S534A mice. However, the number of osteoclasts in the S534A-OVX mice was similar to that in the WT-OVX mice (Fig. 5A and B). Consistent with the in vivo results, there was no significant difference in osteoclast formation induced by M-CSF and RANKL in bone marrow cells derived from WT-Sham, WT-OVX, and S534A-Sham, KI-OVX mice (data not shown). The bone-resorbing activity of osteoclasts was slightly enhanced in S534A-OVX mice (Fig. 5B). This slight promotion of bone resorption activity in S534A-OVX mice was confirmed by measuring CTX-1 levels in serum (Fig. 5C).

We performed double labeling with calcein and alizarin red to evaluate the bone formation rate. There was no significant difference in

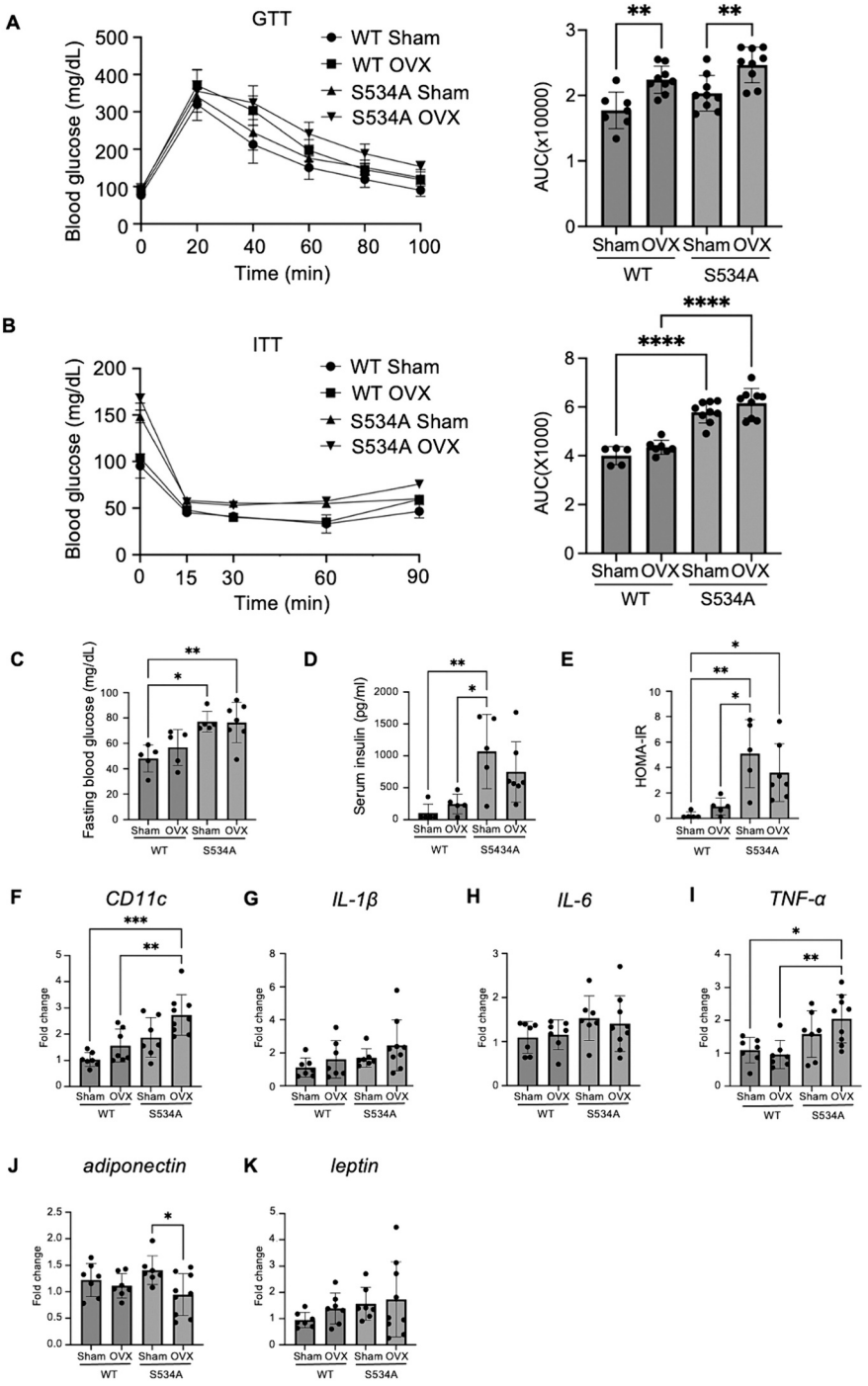

Fig. 3. Capacity of glucose utilization and insulin sensitivity in S534A mice after OVX surgery. **A, B.** IPGTT (A) and ITT (B) and each area under the curve (AUC) data in WT and S534A mice 3 or 4 weeks after Sham or OVX, respectively (n = 5–9/ each group). **C–E.** Fasting serum glucose concentrations (C), fasting serum insulin concentrations (D), and HOMA-IR index (E) in WT and S534A mice 4 weeks after Sham or OVX (n = 5–7). **F–K.** Reverse transcription-quantitative PCR (RT-qPCR) analysis of CD11c (F), IL1β (G), IL6 (H), TNFα (I), adiponectin (J), and leptin (K) in the pgWAT of WT and S534A mice 4 weeks after Sham or OVX (n = 7–9). β-actin was used as an internal control. All values are shown as the means ± SD. Statistical analysis was performed using two-way ANOVA followed by Tukey's post hoc test. $^{*}P < 0.05$, $^{**}P < 0.01$, $^{***}P < 0.001$, $^{****}P < 0.0001$.

the width of labeling between WT-Sham and S534A-Sham mice (Fig. 5D). Since bone metabolism changes to a high turnover type, which increases bone formation after OVX [37,38], the label width increased in WT-OVX mice, but there was no significant difference in label width from the sham group in S534A-OVX mice (Fig. 5D, E). The results of bone morphometry also showed that in WT-OVX mice, the mineral deposition rate (MAR) tended to increase compared to that in WT-Sham mice, and the mineralized surface/bone surface (MS/BS) and bone formation rate (BFR) were enhanced; however, the bone formation parameters of S534A-OVX mice were comparable to those of S534A-Sham mice (Fig. 5E). These results indicated that the decrease in OVX-induced trabecular bone density in S534A mice was due to the suppression of bone formation.

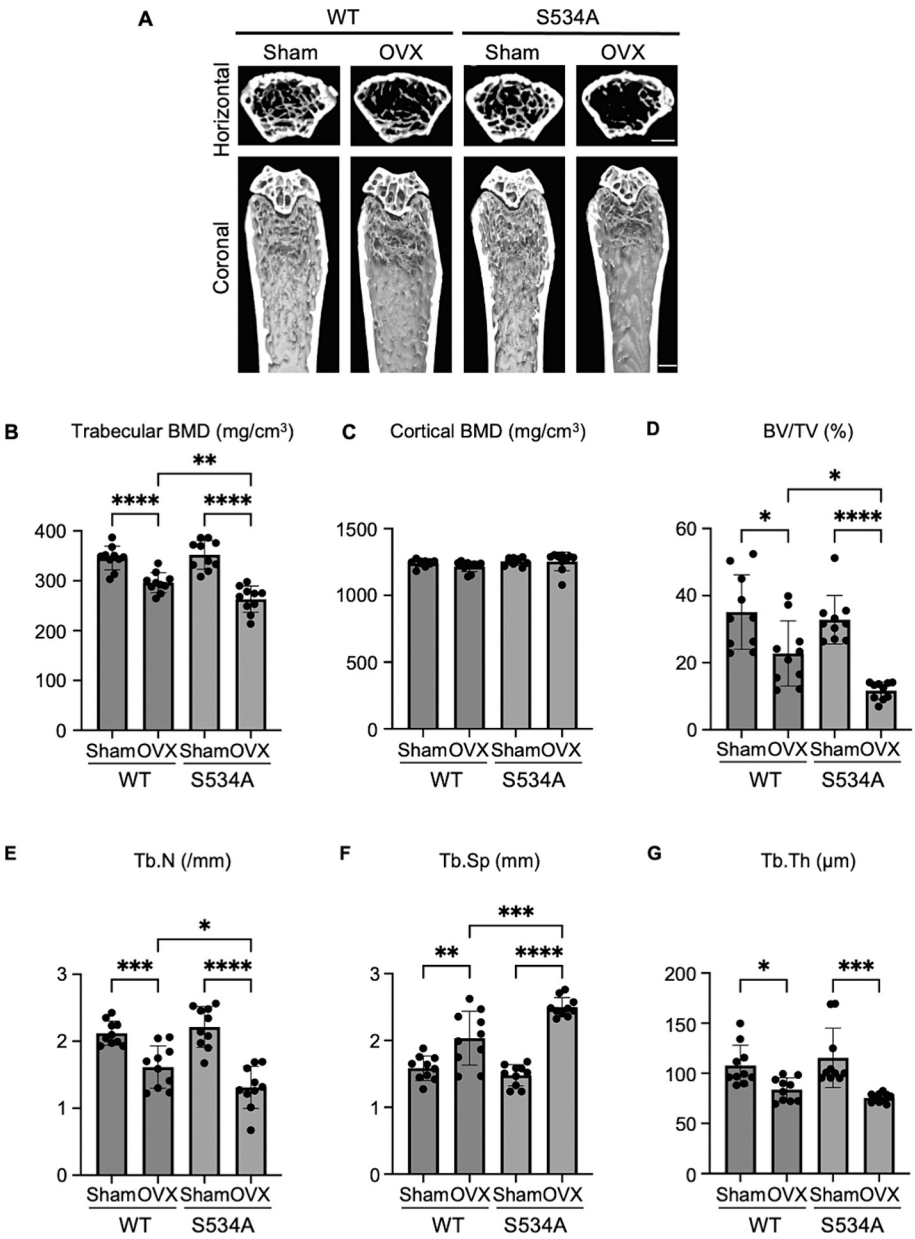

Fig. 4. Bone loss after OVX in S534A mice caused by suppression of bone formation. **A.** Sham or OVX surgery was performed on 9-week-old female WT and S534A mice, and 4 weeks later, the three-dimensional structure of the femur was analyzed using three dimensional (3D)-μCT. Representative 3D-μCT images of the distal regions of femurs of mice. Scale bar = 1 mm. **B–G.** Trabecular bone mineral density (BMD), cortical BMD, bone volume/tissue volume (BV/TV), trabecular number (Tb.N), trabecular separation (Tb.Sp) and trabecular thickness (Tb.Th) in the distal femur regions of mice was quantified using 3D-μCT. Data are presented as the mean ± SD ($n = 10$). All values are shown as the means ± SD. Statistical analysis was performed using two-way ANOVA followed by Tukey's post hoc test. $^{*}P < 0.05$, $^{**}P < 0.01$, $^{***}P < 0.001$, $^{****}P < 0.0001$.

3.5. Determination of osteoblast and adipocyte cell fate by NF-κB activation

Histological analysis also showed Oil Red O staining confirmed that the number of bone marrow adipocytes was higher in the S534A-OVX mice than in the WT-OVX mice (Fig. 6A). Therefore, bone marrow mesenchymal stem cells (BMSCs) were prepared from the bone marrow of WT-Sham, WT-OVX, S534A-Sham, and S534A-OVX mice, and their ability to differentiate into osteoblasts and adipocytes was examined. The number of ALP-positive cells and ALP activity increased in OVX groups compared to cells from Sham groups, but both ALP-positive cell number and ALP activity were lower in BMSCs derived from S534A than those of WT mice (Fig. 6B and C). Similar results were obtained after culturing for 3 weeks and examining calcification, as determined by Alizarin Red S staining (Fig. 6D and E).

In contrast, adipocyte differentiation of BMSCs from S534A mice was enhanced compared with that of WT mice, accompanied by adiponectin expression (Fig. 6F–H), suggesting that BMSCs from S534A mice were more likely to differentiate into adipocytes. These results suggested that the degree of NF-κB activation determines osteoblast and adipocyte differentiation.

3.6. Inhibitory effects of disulfiram on weight gain and bone loss by inhibiting NF-κB activity in femur and adipose tissue after OVX-surgery

DSF, an aldehyde dehydrogenase (ALDH) inhibitor, is a clinically safe drug that has been used to treat alcohol dependence for over 60 years [26]. DSF suppresses NF-κB in various cell types and exhibits new

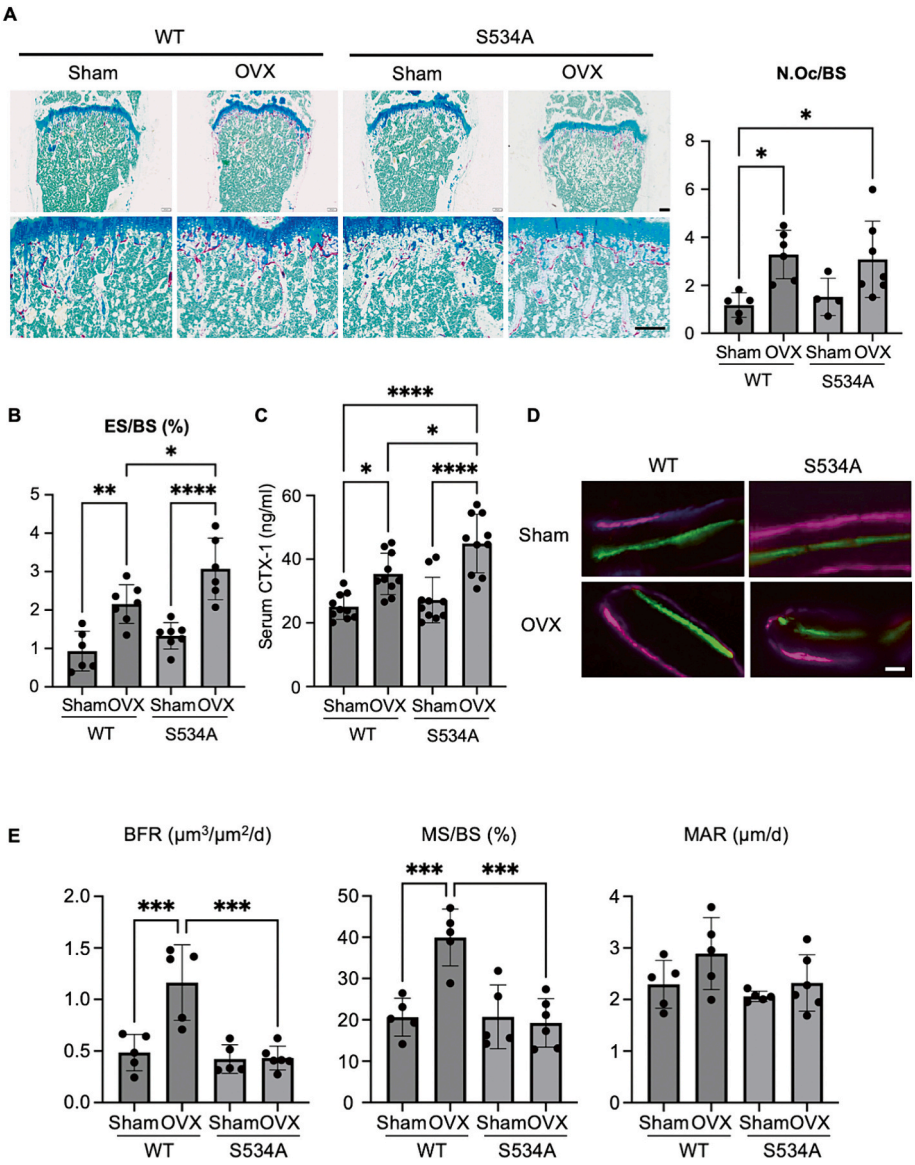

Fig. 5. Further bone loss after OVX in S534A mice by suppressing of bone formation. **A.** Representative images of TRAP staining of the distal regions of femurs of mice. Scale bar = 200 μm. Quantification of osteoclast number/bone surface (N.Oc/BS) in the distal regions of femurs of mice. Data are presented as the mean ± SD (n = 4–7). **B.** Quantification of eroded surface/bone surface (ES/BS) in the distal regions of femurs of mice (n = 6–7). **C.** The amount of CTX-1 in serum in mice was measured using an ELISA kit (n = 10). Data are presented as the mean ± SD. **D.** Administration of calcein (20 mg/kg) and alizarin red S (20 mg/kg) to all mice at 10 and 2 days before euthanasia, with labeling observed using frozen sections. Representative images of calcein and alizarin red S double labeling. Scale bar = 10 μm. **E.** Histomorphometric analyses were performed in the trabecular bone of the femur. Bone formation rate (BFR), mineralized surface/bone surface (MS/BS), and mineral apposition rate (MAR) in the distal regions of femurs of mice. All values are shown as the means ± SD (n = 5–6). Statistical analysis was performed using two-way ANOVA followed by Tukey's post hoc test. *$P < 0.05$, **$P < 0.01$, ***$P < 0.001$, ****$P < 0.0001$.

physiological functions, such as anti-cancer and anti-obesity effects in vivo [23,25]. Therefore, OVX was performed on female NF-κB reporter mice, DSF (50 mg/kg) was subcutaneously administered daily, and NF-κB activation was analyzed 1 week later. DSF suppressed OVX-induced activation of NF-κB in the metaphyses of long bones and WAT (Fig. 7A). Next, female WT mice were subjected to OVX, and DSF (50 mg/kg) was administered subcutaneously every 2 days to measure body weight and examine bone loss over a 4-week period. DSF suppressed OVX-induced weight gain (Fig. 7B). As loss of appetite may occur as a side effect of DSF, we compared the amount of food intake between the sham, OVX, and DSF-treated groups; however, there was no significant difference among the three groups (Fig. 7C). Although OVX-induced weight gain was due to changes in the weight of pgWAT, DSF treatment suppressed the weight of pgWAT, such that it was almost the same as that in the sham group (Fig. 7D). Finally, three-dimensional bone analysis was performed using μCT, and the bone density decreased in the OVX group, but the reduction was suppressed in the DSF group (Fig. 7E). Based on these results, DSF suppressed both postmenopausal weight gain and bone loss.

4. Discussion

ER signaling suppresses NF-κB activation; however, when and where postmenopausal estrogen deficiency activates NF-κB signaling have been unclear [9,10]. Therefore, we established NF-κB reporter mice to observe NF-κB activation in vivo. When the luminescence intensity was measured by shortening the time until measurement after OVX, an enhancement in luminescence intensity was observed at the metaphyses of long bones and pgWAT 1 week after OVX. It is unclear why NF-κB is activated in two separate organs, the bone and adipose tissue. Humoral

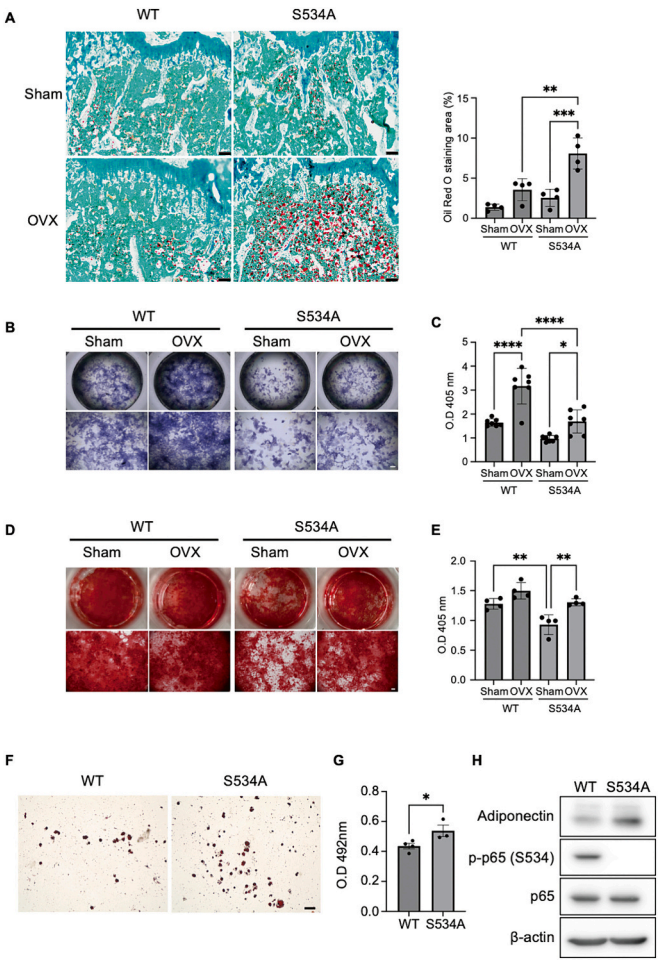

Fig. 6. Regulation of osteoblast differentiation and adipocyte differentiation from bone marrow stem cells by activation of NF-κB. **A.** Representative images of Oil red O staining of the distal regions of femurs of female WT or S534A mice 4 weeks after sham or OVX surgery. Scale bar = 100 μm. Quantification of Oil red O-positive area (per field) in the distal regions of femurs of mice (n = 4). **B.** Bone marrow mesenchymal stem cells (BMSCs) isolated from femurs and tibiae of female WT or S534A mice 4 weeks after sham or OVX surgery, were treated with β-glycerophosphate (β-GP) (10 mM) and ascorbic acid (A.A) (50 μg/mL). Alkaline phosphatase (ALP) staining BMCs cultured for 7 days. Scale bar = 200 μm. **C.** ALP activity quantitation of BMSCs cultured for 7 days (n = 7). **D.** Mineralization staining of BMSCs with Alizarin Red S on day 21. **E.** Quantification of the stained mineral layers in cultured BMSCs (n = 4). Scale bar = 200 μm. **F.** Isolated BMSCs from 4-week-old female WT or S534A mice were treated with dexamethasone (1 μM), troglitazone (10 μM), insulin (10 μg/mL), and IBMX (0.5 mM) for 6 days. The cells were stained for Oil red O staining. Scale bar = 100 μm. **G.** Quantification of Oil red O dye. Oil red-O dye was extracted from 100 % isopropyl alcohol and its absorbance was measured at 492 nm using SpectraMax iD3 (Molecular Devices) (n = 3–4). All values are shown as the means ± SD. Statistical analysis between two groups was performed using unpaired t-test. **H.** Immunoblot analysis was used to determine of adiponectin, phospho-p65 (S534), and total p65. β-Actin was used as a loading control. All values are shown as the means ± SD. Statistical analysis was performed using two-way ANOVA followed by Tukey's post hoc test. $^{*}P < 0.05$, $^{**}P < 0.01$, $^{***}P < 0.001$, $^{****}P < 0.0001$.

factors flowing in the blood may activate NF-κB in these two organs. Estrogen deficiency increases the expression of inflammatory cytokines such as IL-1, IL-6, and TNF-α [4,39]. Furthermore, it has been reported that OVX mice have increased amounts of soluble RANKL, which is essential for osteoclast differentiation [11]. It is likely that these ligands, rather than a single molecule, work together to activate NF-κB in long bones and pgWAT. It is also important to clarify in which cells NF-κB is activated in long bone metaphysis and pgWAT. After OVX, there is a tendency for CD11c-positive macrophages to increase in pgWAT, and osteoclasts differentiate from macrophages, whereas osteoblasts and adipocytes differentiate from common mesenchymal stem cells, which exist in both the bone marrow and adipose tissue [7]. It is important to perform OVX in macrophage- or mesenchymal stem cell-specific RelA-deficient mice and examine whether bone loss and weight gain occur.

NF-κB function is partly regulated by post-translational modifications of the RelA subunit, such as phosphorylation and acetylation [19,20]. It has been reported that extracellular stimulation renews the stabilization of RelA protein in MEFs derived from S534A mice, promoting transcriptional activity [22]. However, whether NF-κB activation is enhanced in vivo remained unknown. Thus, we crossed NF-κB reporter mice with S534A mice, excised the bone and WAT 1 week after OVX, and measured NF-κB activity ex vivo. Compared to NF-κB reporter mice, S534A/NF-κB reporter mice had enhanced activation of NF-κB in bone and WAT 1 week after OVX. Furthermore, when WT and S534A mice were subjected to OVX, there was no difference in weight gain (although S534A mice gained more weight than WT mice at 21 weeks of age) or bone loss in the sham group; however, S534A mice showed increased weight gain and bone loss in the OVX group. Most of the NF-κB-activated mice used so far are transgenic mice overexpressing constitutively active IKKβ in a tissue-specific manner [40,41]. Since the phenotype is observed simply by expressing constitutively active IKKβ in these mice, S534A mice may be useful for examining stimulus-dependent phenotypes.

Weight gain due to estrogen deficiency is caused by an effect on the hypothalamus, poor control of the feeding and satiety center, changes in adipose tissue energy homeostasis, and adipokine production; however, there is no consensus on the same [1–3]. In this study, there was no significant difference in food intake among the four groups of WT and S534A mice. The relationship between NF-κB activation, obesity, and carbohydrate/lipid metabolism has been well studied [10,16–18]. In mice where NF-κB activation is specifically suppressed in the hypothalamus, liver, adipose tissue, and muscle involved in energy metabolism, obesity and deterioration of glucose tolerance caused by HFD are generally suppressed [10,16–18]. Transgenic mice that express a constitutively active form of IKKβ in the liver promote fat synthesis by regulating molecules involved in lipogenesis and cholesterol synthesis at the post-translational level [41]. However, in transgenic mice overexpressing constitutively active IKKβ in adipose tissue under the control of the aP2 promoter, the transcriptional activity of NF-κB in adipose tissue is enhanced compared to WT mice, which results in increased adipose tissue inflammation and food intake. Nevertheless, owing to the high metabolic rate, there was no weight gain or increase in the adipose tissue weight, and glucose tolerance improved [42]. Although the discrepancy between these results and ours cannot be explained, hyperactivation of NF-κB by overexpression by constitutively active IKKβ also may induce the expression of genes that enhance energy metabolism, such as lipolysis, rather than the expression of genes that promote fat synthesis.

Central obesity in postmenopausal women is thought to be an early-stage disease associated with metabolic syndrome (MetS) [3]. Visceral adipose tissue contains adipocytokines such as leptin and resistin, as well as inflammatory cytokines such as IL-6 and TNF-α, and thrombogenic factors such as plasminogen activator inhibitor 1 (PAI-1) [3]. The body weight of S534A mice increased compared with that of WT mice in the OVX group and that of 21-week-old mice in the sham group. In addition, the pgWAT/body weight of S534A mice was higher than that of WT mice (Fig. 2). Additionally, increased expression of TNF-α and subsequent insulin resistance were observed in S534A mice. In general, the prevalence of MetS is higher in men than in premenopausal women of the same age; however, the trend in MetS prevalence is reversed during menopause, with the prevalence being higher in women than in men [43]. Weight gain and worsening of glucose tolerance due to postmenopausal NF-κB activation may trigger MetS in women.

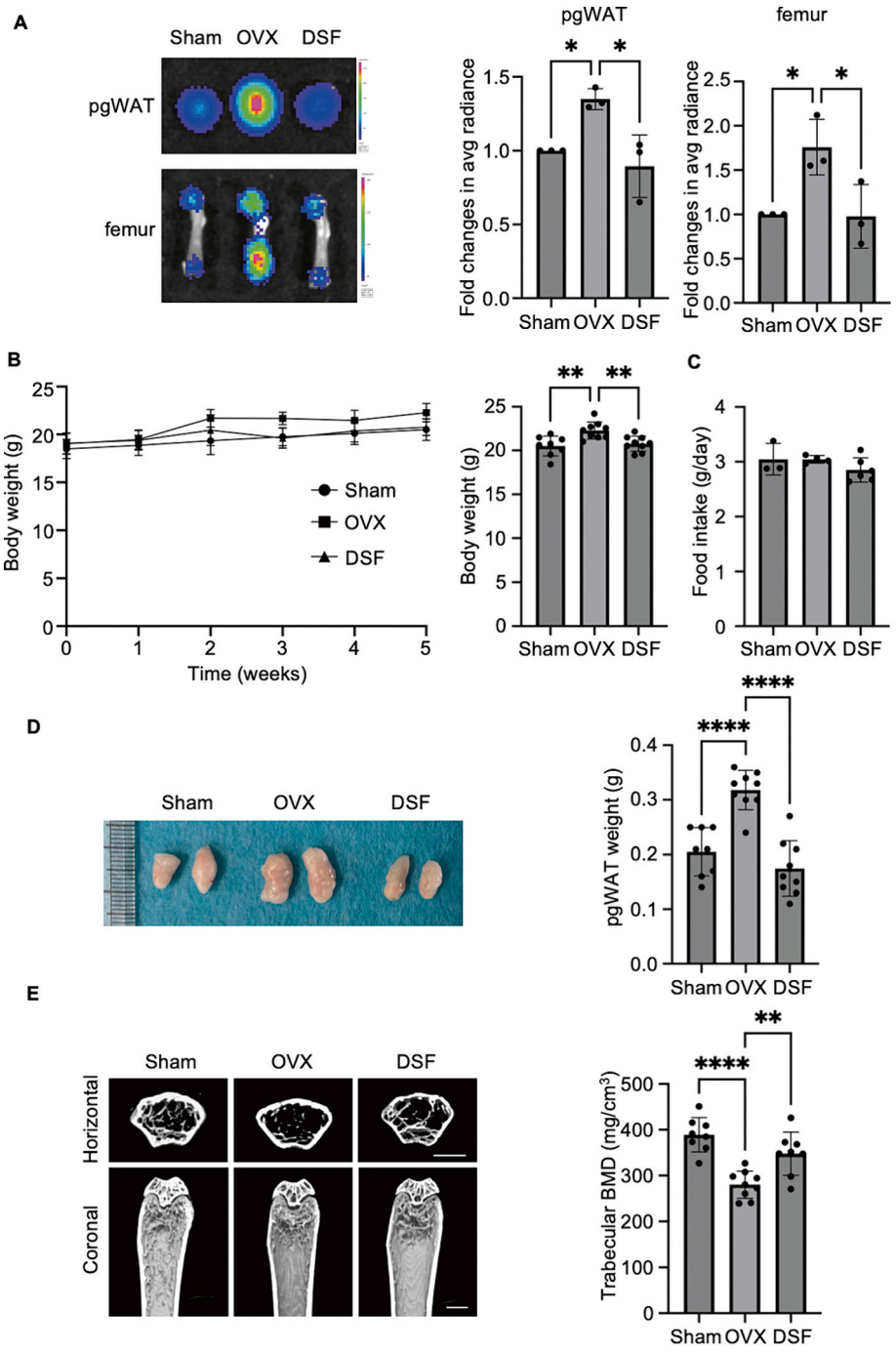

Fig. 7. Inhibitory effects of disulfiram on weight gain and bone loss after OVX surgery. **A.** Nine-week-old female NF-κB reporter mice were subjected to sham or OVX surgery, and DSF (50 mg/kg) administered via subcutaneous injection every day. One week later, D-luciferin (150 mg/kg) was administered intraperitoneally, and the bioluminescence images of the pgWAT and femur was captured. Luminescence intensity was quantified and express as fold change (n = 3). **B.** OVX mice were administered DSF for 4 weeks by subcutaneous injection every 2 days. (1) Sham group (Sham operation + DMSO in Propylene Glycol, $n = 8$), (2) vehicle group (OVX + DMSO in Propylene Glycol, $n = 9$), (3) DSF group (OVX + DSF 50 mg/kg, n = 9). Growth curves (B) and body weight at 4 weeks after control/DSF treatment. **C.** Food intake of the three groups. **D.** Representative appearance of the pgWAT and pgWAT weight of the three groups. **E.** Representative 3D-μCT images of the distal regions of femurs of the three groups. Scale bar = 1 mm. Trabecular bone mineral density (BMD) of the distal regions of femurs of mice the three groups were measured by 3D-μCT. Data are expressed as the mean ± SD (n = 8–9). All values are shown as the means ± SD. Statistical analysis was performed using two-way repeated measures ANOVA (B), one-way ANOVA followed by Tukey's post hoc test (C, D, E). $^{*}P < 0.05$, $^{**}P < 0.01$, $^{***}P < 0.001$, $^{****}P < 0.0001$.

Postmenopausal osteoporosis decreases bone mass due to increased bone resorption rather than bone formation; thus, estrogen is thought to suppress bone resorption [1–5]. Either pharmacological or genetic suppression of NF-κB also inhibits osteoclast formation [7,12,13,44] and promotes osteoblast formation [7,45–47]. Meanwhile, transgenic mice that activate NF-κB by overexpressing the constitutive active of IKKβ promote bone resorption [48] and suppress bone formation [49] in vivo, thereby decreasing in bone mass. Collectively, these results suggest that activation of NF-κB enhances bone resorption and suppresses bone formation thereby decreasing bone mass, whereas inhibition of NF-κB has the opposite effect. As expected, OVX-induced bone loss was accelerated in S534A mice, but there was no change in the number of osteoclasts

compared to WT mice; bone-resorbing activity was only slightly enhanced, but bone formation was significantly suppressed. This result is not simply caused by enhanced activation of NF-κB in S534A mice but may also be due to a structural change in RelA caused by the S534A mutation. There are few reports on human RelA mutations in bone diseases; however, a heterozygous de novo missense mutation (c.1534_1535delinsAG, p. Asp512Ser) has been observed [50]. This missense change suppresses the activation of NF-κB, and although it is expressed throughout the body, it is not due to osteoclast dysfunction, but neonatal bone sclerosis caused by hyperactivity of osteoblasts in the uterus [50]. Thus, there may be a special molecular mechanism by which RelA mutations act only on osteoblasts.

Rather than developing new drugs, we proposed drug repositioning with those that are currently considered safe in clinical practice. DSF was selected as a candidate drug based on three criteria: inhibition of NF-κB activation [23], inhibition of bone loss in bone disease models [24], and improvement of obesity and energy metabolism [25]. As expected, DSF suppressed OVX-induced NF-κB activation in vivo and further suppressed weight gain and bone loss. On the other hand, it has been reported that bone formation is suppressed in ALDH2-deficient mice [51], or when DSF is administered to WT mice [52]. Although the contradiction with the results of this study has not been resolved, bone resorption is relatively enhanced in the case of the OVX model; thus, the bone resorption inhibitory effect of DSF may be more pronounced. Since the main cause of osteoporosis due to aging is the suppression of bone formation, it may be necessary to be careful when administering DSF.

To date, NCBI has published 74 human clinical studies of DSF for various conditions, including alcohol and cocaine use disorders ($n = 36$), cancer ($n = 26$), and HIV ($n = 5$) (https://www.clinicaltrials.gov/). However, its application to “osteoporosis” and “bone loss” has not been described although one application for “obesity” has been registered, even though the details are unknown. In recent years, the number of indications for cancer treatment has increased, and it has been reported that it inhibits NPL4, an adapter for segregase [53], and FROUNT, which is involved in the regulation of macrophage function [54]. Our results do not indicate that the effects of DSF are related to ALDH2 inhibition, which is thought to be the mechanism of action for the treatment of chronic alcohol dependence. When considering DSF as a treatment for postmenopausal osteoporosis and weight gain, it is necessary to consider the possibility that it and its metabolites may cause adverse reactions to alcohol intake.

In conclusion, activation of NF-κB may be a therapeutic target for postmenopausal weight gain and bone loss, and DSF is one of its promising drugs.

Supplementary data to this article can be found online at https://doi.org/10.1016/j.bbadis.2024.167320.

CRediT authorship contribution statement

Fei Huang: Writing – review & editing, Writing – original draft, Validation, Investigation, Funding acquisition, Formal analysis, Data curation. **Jing Gao:** Writing – review & editing, Writing – original draft, Supervision, Formal analysis, Data curation. **Aonan Li:** Writing – review & editing, Investigation, Formal analysis, Data curation. **Akiko Mizokami:** Writing – review & editing, Supervision, Methodology. **Miho Matsuda:** Writing – review & editing, Methodology. **Kazuhiro Aoki:** Writing – review & editing, Supervision, Investigation, Formal analysis. **Takenobu Katagiri:** Writing – review & editing, Validation, Supervision. **Tomoyo Kawakubo-Yasukochi:** Writing – review & editing, Writing – original draft, Supervision, Formal analysis, Conceptualization. **Eijiro Jimi:** Writing – review & editing, Writing – original draft, Validation, Resources, Conceptualization.

Declaration of competing interest

The authors have declared no conflict of interest.

Data availability

Data will be made available on request.

Acknowledgment

The authors thank Mr. Hiroshi Otowa for their technical assistance in data collection of histology. We would like to thank Editage (www.editage.com) for English language editing. This study was supported by SPRING Program Future-Creation (MIRAI) Course to F.H. (JPMJSP2136), and Japan Society for the Promotion of Science (JSPS) KAKENHI grants (18H02967, and 21H03108 to E.J.).

References

[1] G. Stachowiak, T. Pertynski, M. Pertynska-Marczewska, Metabolic disorders in menopause, Prz Menopauzalny 14 (2015) 59–64.
[2] H.G. Jeong, H. Park, Metabolic disorders in menopause, Metabolites 12 (2022) 954.
[3] R.A. Lobo, A. Gompel, Management of menopause: a view towards prevention, Lancet Diabetes Endocrinol. 10 (2022) 457–470.
[4] J. Pfeilschifter, R. Köditz, M. Pfohl, H. Schatz, Changes in proinflammatory cytokine activity after menopause, Endocr. Rev. 23 (2002) 90–119.
[5] I. Paterni, C. Granchi, J.A. Katzenellenbogen, F. Minutolo, Estrogen receptors alpha (ERα) and beta (ERβ): subtype-selective ligands and clinical potential, Steroids 90 (2014) 13–29.
[6] R.G. Baker, M.S. Hayden, S. Ghosh, NF-κB, inflammation, and metabolic disease, Cell Metab. 13 (2011) 11–22.
[7] E. Jimi, N. Takakura, F. Hiura, I. Nakamura, S. Hirata-Tsuchiya, The role of NF-κB in physiological bone development and inflammatory bone diseases: is NF-κB inhibition “killing two birds with one stone”? Cells 8 (2019) 1636.
[8] D. Capece, D. Verzella, I. Flati, P. Arboretto, J. Cornice, G. Franzoso, NF-κB: blending metabolism, immunity, and inflammation, Trends Immunol. 43 (2022) 757–775.
[9] D. Kalaitzidis, T.D. Gilmore, Transcription factor cross-talk: the estrogen receptor and NF-κB, Trends Endocrinol. Metab. 16 (2005) 46–52.
[10] D.K. Biswas, S. Singh, Q. Shi, A.B. Pardee, J.D. Iglehart, Crossroads of estrogen receptor and NF-κB signaling, Sci. STKE 2005 (2005) pe27.
[11] C. Streicher, A. Heyny, O. Andrukhova, B. Haigl, S. Slavic, C. Schuler, et al., Estrogen regulates bone turnover by targeting RANKL expression in bone lining cells, Sci. Rep. 7 (2017) 6460.
[12] Y. Zhang, H. Guan, J. Li, Z. Fang, W. Chen, F. Li, Amlexanox suppresses osteoclastogenesis and prevents ovariectomy-induced bone loss, Sci. Rep. 5 (2015) 13575.
[13] N. Takakura, M. Matsuda, M. Khan, F. Hiura, K. Aoki, Y. Hirohashi, et al., A novel inhibitor of NF-κB-inducing kinase prevents bone loss by inhibiting osteoclastic bone resorption in ovariectomized mice, Bone 135 (2020) 115316.
[14] T. Aoki, F. Hiura, A. Li, N. Yang, N. Takakura-Hino, S. Mukai, et al., Inhibition of non-canonical NF-κB signaling suppresses periodontal inflammation and bone loss, Front. Immunol. 14 (2023) 1179007.
[15] E. Jimi, K. Aoki, H. Saito, F. D'Acquisto, M.J. May, I. Nakamura, et al., Selective inhibition of NF-κB blocks osteoclastogenesis and prevents inflammatory bone destruction in vivo, Nat. Med. 10 (2004) 617–624.
[16] X. Zhang, G. Zhang, H. Zhang, M. Karin, H. Bai, D. Cai, Hypothalamic IKKβ/NF-κB and ER stress link overnutrition to energy imbalance and obesity, Cell 135 (2008) 61–73.
[17] M.C. Arkan, A.L. Hevener, F.R. Greten, S. Maeda, Z.W. Li, J.M. Long, A. Wynshaw-Boris, G. Poli, J. Olefsky, M. Karin, IKK-β links inflammation to obesity-induced insulin resistance, Nat. Med. 11 (2005) 191–198.
[18] H. Kwon, S. Laurent, Y. Tang, H. Zong, P. Vemulapalli, J.E. Pessin, Adipocyte-specific IKKβ signaling suppresses adipose tissue inflammation through an IL-13-dependent paracrine feedback pathway, Cell Rep. 9 (2014) 1574–1583.
[19] A. Oeckinghaus, S. Ghosh, The NF-κB family of transcription factors and its regulation, Cold Spring Harb. Perspect. Biol. 1 (2009) a000034.
[20] F. Christian, E.L. Smith, R.J. Carmody, The regulation of NF-κB subunits by phosphorylation, Cells 5 (2016) 12.
[21] M. Milanovic, M. Kracht, M.L. Schmitz, The cytokine-induced conformational switch of nuclear factor κB p65 is mediated by p65 phosphorylation, Biochem. J. 457 (2014) 401–413.
[22] J.P. Pradere, C. Hernandez, C. Koppe, R.A. Friedman, T. Luedde, R.F. Schwabe, Negative regulation of NF-κB p65 activity by serine 536 phosphorylation, Sci. Signal. 9 (2016) ra85.
[23] Y. Jiao, B.N. Hannafon, W.Q. Ding, Disulfiram’s anticancer activity: evidence and mechanisms, Anticancer Agents Med Chem. 16 (2016) 1378–1384.

[24] H. Ying, A. Qin, T.S. Cheng, N.J. Pavlos, S. Rea, K. Dai, M.H. Zheng, Disulfiram attenuates osteoclast differentiation in vitro: a potential antiresorptive agent, PloS One 10 (2015) e0125696.
[25] M. Bernier, S.J. Mitchell, D. Wahl, A. Diaz, A. Singh, W. Seo, et al., Disulfiram treatment normalizes body weight in obese mice, Cell Metab. 32 (2020) 203–214 e204.
[26] E. Jacobsen, O. Martensen-Larsen, Treatment of alcoholism with tetraethylthiuram disulfide (antabuse), JAMA 139 (1949) 918–922.
[27] T. Kawamoto, Use of a new adhesive film for the preparation of multi-purpose fresh-frozen sections from hard tissues, whole-animals, insects and plants, Arch. Histol. Cytol. 66 (2003) 123–143.
[28] D.W. Dempster, J.E. Compston, M.K. Drezner, F.H. Glorieux, J.A. Kanis, H. Malluche, et al., Standardized nomenclature, symbols, and units for bone histomorphometry: a 2012 update of the report of the ASBMR Histomorphometry Nomenclature Committee, J. Bone Miner. Res. 28 (2013) 2–17.
[29] S. Dagdeviren, M.F. Hoang, M. Sarikhani, V. Meier, J.C. Benoit, M.C. Okawa, et al., An insulin-regulated arrestin domain protein controls hepatic glucagon action, J. Biol. Chem. 299 (2023) 105045.
[30] K. Minowa, D. Rodriguez-Agudo, M. Suzuki, Y. Muto, S. Hirai, Y. Wang, et al., Insulin dysregulation drives mitochondrial cholesterol metabolite accumulation: initiating hepatic toxicity in nonalcoholic fatty liver disease, J. Lipid Res. 64 (2023) 100363.
[31] K. Touyama, M. Khan, K. Aoki, M. Matsuda, F. Hiura, N. Takakura, et al., Bif-1/Endophilin B1/SH3GLB1 regulates bone homeostasis, J. Cell. Biochem. 120 (2019) 18793–18804.
[32] J. Gao, R. Muroya, F. Huang, K. Nagata, M. Shin, R. Nagano, et al., Bone morphogenetic protein induces bone invasion of melanoma by epithelial-mesenchymal transition via the Smad1/5 signaling pathway, Lab. Invest. 101 (2021) 1475–1483.
[33] A. Kumar, K. Sundaram, J. Mu, G.W. Dryden, M.K. Sriwastva, C. Lei, et al., High-fat diet-induced upregulation of exosomal phosphatidylcholine contributes to insulin resistance, Nat. Commun. 12 (2021) 213.
[34] A. Yadav, M.A. Kataria, V. Saini, A. Yadav, Role of leptin and adiponectin in insulin resistance, Clin. Chim. Acta 417 (2013) 80–84.
[35] R. Ahmad, A. Al-Roub, S. Kochumon, N. Akther, R. Thomas, M. Kumari, et al., The synergy between palmitate and TNF-α for CCL2 production is dependent on the TRIF/IRF3 pathway: implications for metabolic inflammation, J. Immunol. 200 (2018) 3599–3611.
[36] J.K. Sethi, G.S. Hotamisligil, Metabolic messengers: tumour necrosis factor, Nat. Metab. 3 (2021) 1302–1312.
[37] H. Liang, Y. Ma, S. Pun, M. Stimpel, W.S. Jee, Aging- and ovariectomy-related skeletal changes in spontaneously hypertensive rats, Anat. Rec. 249 (1997) 173–180.
[38] A. Takakura, R. Takao-Kawabata, Y. Isogai, M. Kajiwara, H. Murayama, S. Ejiri, et al., Differences in vertebral, tibial, and iliac cancellous bone metabolism in ovariectomized rats, J. Bone Miner. Metab. 34 (2016) 291–302.
[39] M.N. Weitzmann, R. Pacifici, Estrogen deficiency and bone loss: an inflammatory tale, J. Clin. Invest. 116 (2006) 1186–1194.
[40] D. Cai, M. Yuan, D.F. Frantz, P.A. Melendez, L. Hansen, J. Lee, S.E. Shoelson, Local and systemic insulin resistance resulting from hepatic activation of IKK-β and NF-κB, Nat. Med. 11 (2005) 183–190.
[41] A. Heida, N. Gruben, L. Catrysse, M. Koehorst, M. Koster, N.J. Kloosterhuis, et al., The hepatocyte IKK:NF-κB axis promotes liver steatosis by stimulating de novo lipogenesis and cholesterol synthesis, Mol. Metab. 54 (2021) 101349.
[42] P. Jiao, B. Feng, J. Ma, Y. Nie, E. Paul, Y. Li, H. Xu, Constitutive activation of IKKβ in adipose tissue prevents diet-induced obesity in mice, Endocrinology 153 (2012) 154–165.
[43] Y.A. Cho, J. Kim, E.R. Cho, A. Shin, Dietary patterns and the prevalence of metabolic syndrome in Korean women, Nutr. Metab. Cardiovasc. Dis. 21 (2011) 893–900.
[44] G. Shen, X. Liu, W. Lei, R. Duan, Z. Yao, Plumbagin is a NF-κB-inducing kinase inhibitor with dual anabolic and antiresorptive effects that prevents menopausal-related osteoporosis in mice, J. Biol. Chem. 298 (4) (2022 Apr) 101767.
[45] J. Chang, Z. Wang, E. Tang, Z. Fan, L. McCauley, R. Franceschi, et al., Inhibition of osteoblastic bone formation by nuclear factor-κB, Nat. Med. 15 (2009) 682–689.
[46] N. Alles, N.S. Soysa, J. Hayashi, M. Khan, A. Shimoda, H. Shimokawa, et al., Suppression of NF-κB increases bone formation and ameliorates osteopenia in ovariectomized mice, Endocrinology 151 (2010) 4626–4634.
[47] S. Hirata-Tsuchiya, H. Fukushima, T. Katagiri, S. Ohte, M. Shin, K. Nagano, et al., Inhibition of BMP2-induced bone formation by the p65 subunit of NF-κB via an interaction with Smad4, Mol. Endocrinol. 28 (2014) 1460–1470.
[48] J.E. Otero, T. Chen, K. Zhang, Y. Abu-Amer, Constitutively active canonical NF-κB pathway induces severe bone loss in mice, PloS One 7 (2012) e38694.
[49] G. Swarnkar, K. Zhang, G. Mbalaviele, F. Long, Y. Abu-Amer, Constitutive activation of IKK2/NF-κB impairs osteogenesis and skeletal development, PloS One 9 (2014) e91421.
[50] A.L. Frederiksen, M.J. Larsen, K. Brusgaard, D.V. Novack, P.J. Knudsen, H. D. Schroder, et al., Neonatal high bone mass with first mutation of the NF-κB complex: heterozygous de novo missense (p.Asp512Ser) RELA (Rela/p65), J. Bone Miner. Res. 31 (2016) 163–172.
[51] Y. Shimizu, A. Sakai, K. Menuki, T. Mori, T. Isse, T. Oyama, et al., Reduced bone formation in alcohol-induced osteopenia is associated with elevated p21 expression in bone marrow cells in aldehyde dehydrogenase 2-disrupted mice, Bone 48 (2011) 1075–1086.
[52] M. Mittal, K. Khan, S. Pal, K. Porwal, S.P. China, T.K. Barbhuyan, et al., The thiocarbamate disulphide drug, disulfiram induces osteopenia in rats by inhibition of osteoblast function due to suppression of acetaldehyde dehydrogenase activity, Toxicol. Sci. 139 (2014) 257–270.
[53] Z. Skrott, M. Mistrik, K.K. Andersen, S. Friis, D. Majera, J. Gursky, et al., Alcohol-abuse drug disulfiram targets cancer via p97 segregase adaptor NPL4, Nature 552 (2017) 194–199.
[54] Y. Terashima, E. Toda, M. Itakura, M. Otsuji, S. Yoshinaga, K. Okumura, et al., Targeting FROUNT with disulfiram suppresses macrophage accumulation and its tumor-promoting properties, Nat. Commun. 11 (2020) 609.

A

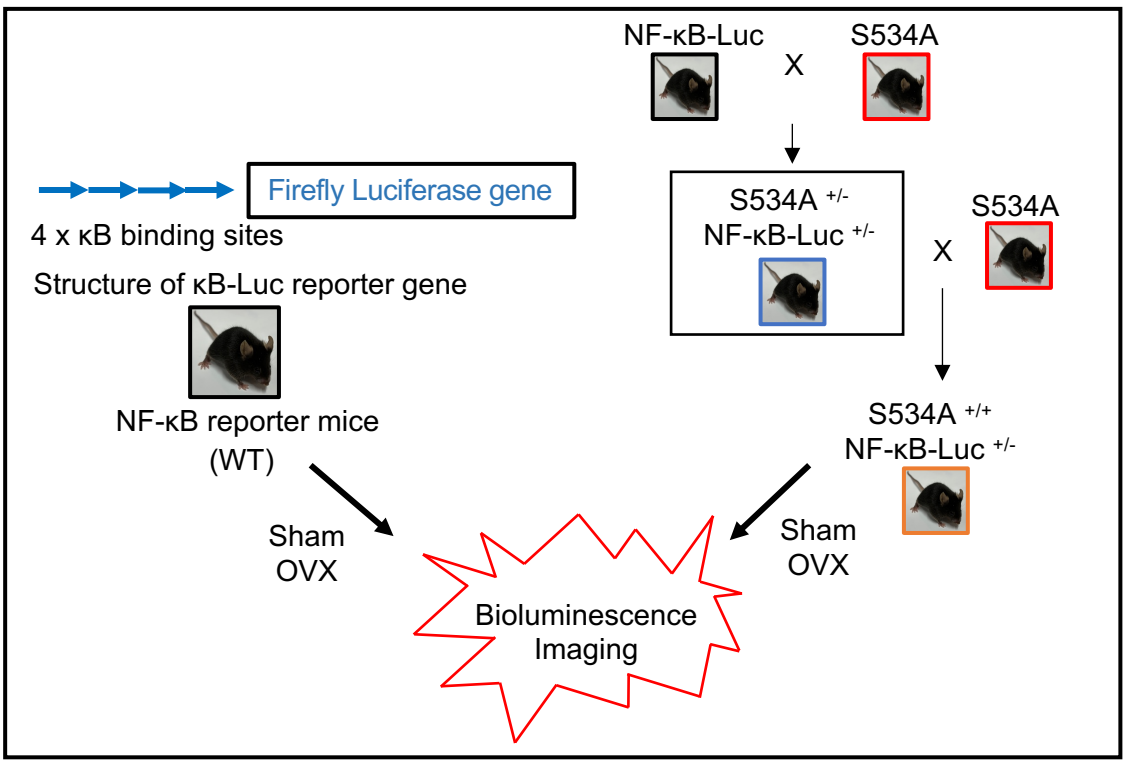

B

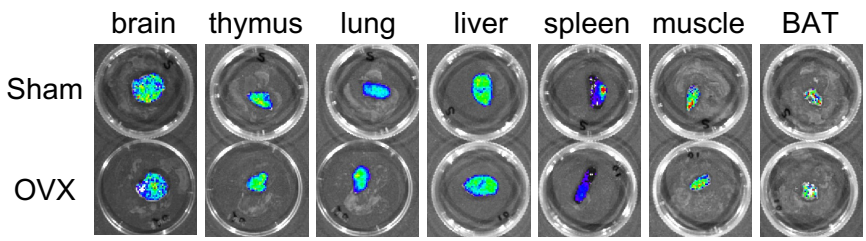

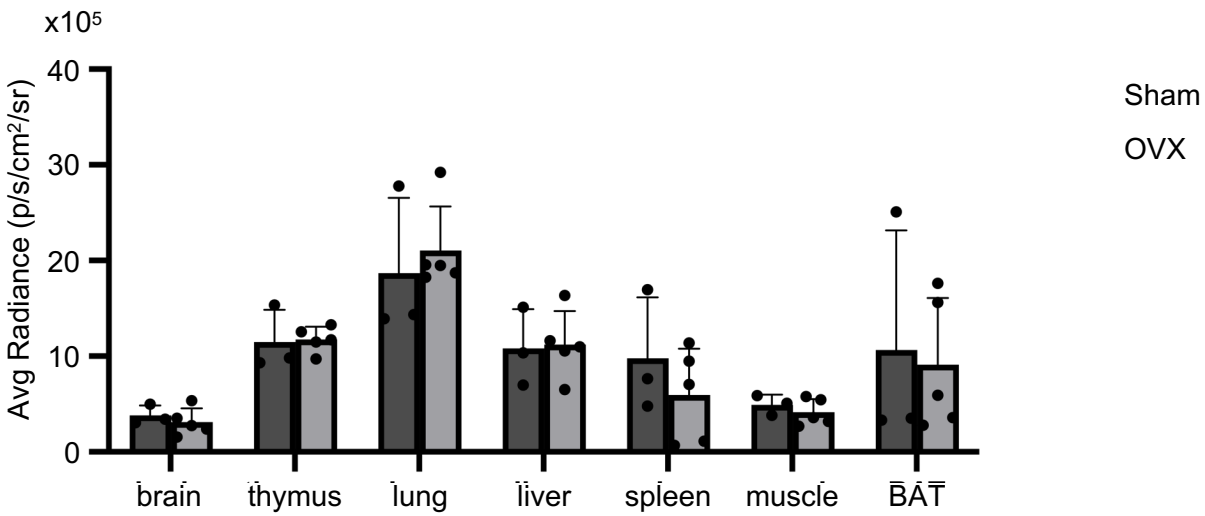

Supplementary Figure 1.

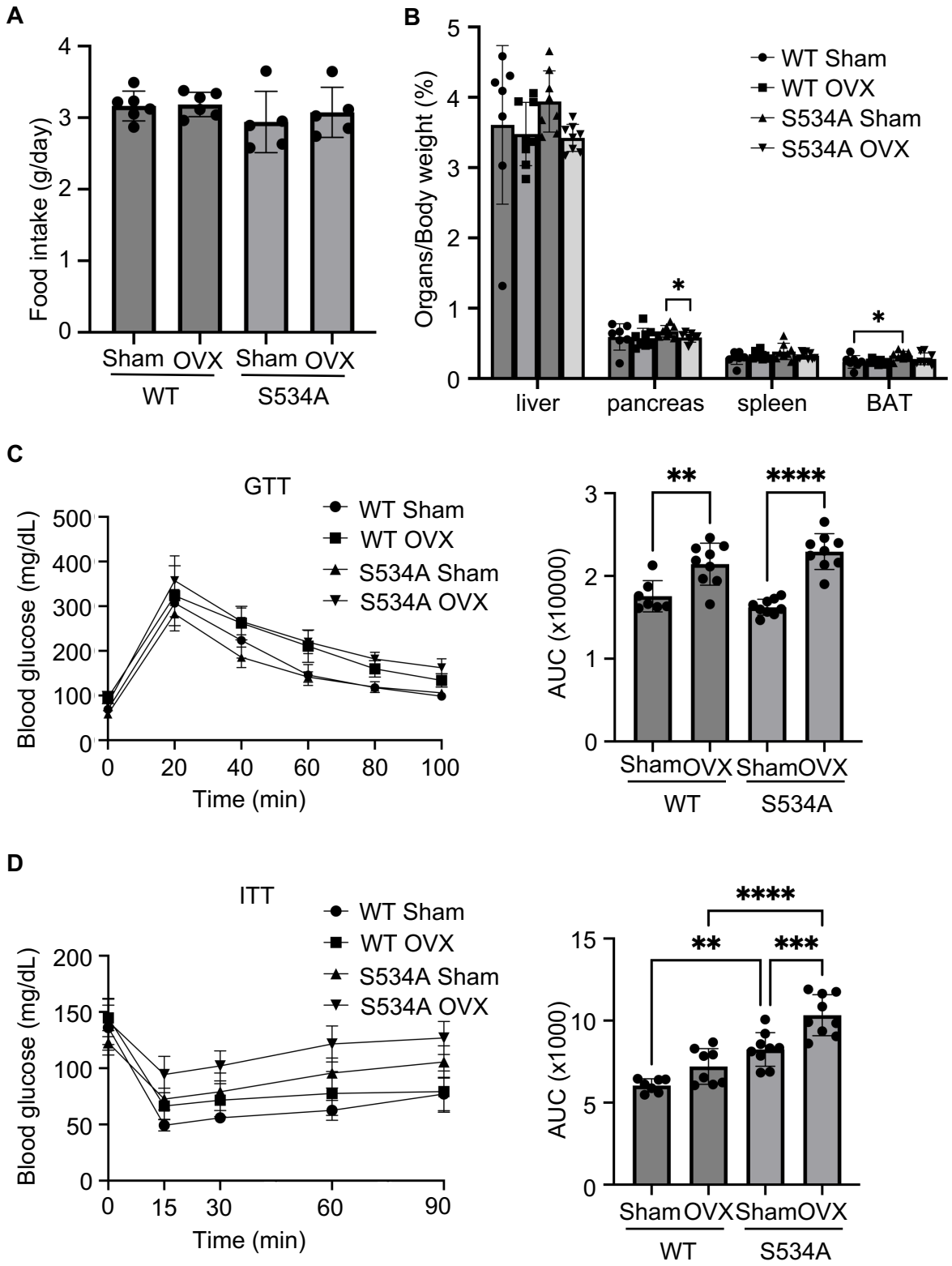

Supplementary Figure 2.